

# Effect of Supercritical Carbon Dioxide on the Thermodynamics of Model Blends of Styrene-Acrylonitrile Copolymer and Poly(methyl methacrylate) Studied by Small-Angle Neutron Scattering

Sebnem Inceoglu,<sup>‡,†</sup> Nicholas P. Young,<sup>‡,†</sup> Andrew J. Jackson,<sup>§</sup> Steven R. Kline,<sup>‡</sup> Stéphane Costeux,<sup>||</sup> and Nitash P. Balsara<sup>‡,○,¶,\*</sup>

<sup>‡</sup>Department of Chemical and Biomolecular Engineering, University of California, Berkeley, California 94720, United States

<sup>§</sup>European Spallation Source ESS AB, Lund, SE-221 00, Sweden

<sup>‡</sup>NIST Center for Neutron Research, Gaithersburg, Maryland 20899-6102, United States

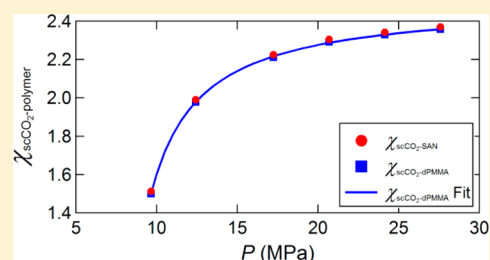
<sup>||</sup>Dow Coatings & Construction, The Dow Chemical Company, Midland, Michigan 48674, United States

<sup>○</sup>Materials Sciences Division, Lawrence Berkeley National Laboratory, Berkeley, California 94720, United States

<sup>¶</sup>Environmental Energy Technologies Division, Lawrence Berkeley National Laboratory, Berkeley, California 94720, United States

## S Supporting Information

**ABSTRACT:** Quantitative analysis of small angle neutron scattering (SANS) data from homogeneous multicomponent mixtures of supercritical carbon dioxide (scCO<sub>2</sub>) and two polymers is presented for the first time. The two polymers used in this study were styrene-acrylonitrile copolymer (SAN) and deuterated poly(methyl methacrylate) (dPMMA). Model polymers were used to facilitate comparisons between theory and experiment. The random phase approximation (RPA) was used to derive a simple expression to describe SANS profiles. The scCO<sub>2</sub>-free binary blend was studied to determine the temperature dependence of the polymer–polymer interaction parameter. scCO<sub>2</sub>-polymer solubility data was used to relate polymer–solvent interaction parameters. Comparisons between SANS profiles from multicomponent mixtures and the RPA expression provided an estimate of the interaction parameter between scCO<sub>2</sub> and PMMA,  $\chi_{13}$ . The addition of scCO<sub>2</sub> at a modest pressure results in a decrease of phase separation temperature  $T_s$  by 127 K. The analysis indicates that the change in  $T_s$  is caused by an increase in  $\chi_{13}$  with increasing scCO<sub>2</sub> pressure.



## 1. INTRODUCTION

Supercritical carbon dioxide (scCO<sub>2</sub>) has been investigated extensively in recent years as an environmentally benign option for the synthesis and processing of polymers.<sup>1</sup> Owing mostly to its accessible critical point (critical temperature  $T_{c,CO_2} = 304.1$  K and critical pressure  $P_{c,CO_2} = 7.38$  MPa), scCO<sub>2</sub> has a unique set of properties which enable its widespread use. Temperature ( $T$ ) and pressure ( $P$ ) can be used to tune the physical properties of scCO<sub>2</sub>, including density, viscosity, and diffusivity, over a wide range of values. One key result of this characteristic is that the solvent quality of scCO<sub>2</sub> with many solutes of practical interest can be adjusted to obtain the desired behavior. The efficacy of scCO<sub>2</sub> for polymer processing has been established in applications including organic photovoltaics,<sup>2</sup> supercapacitors,<sup>3</sup> and foams for various purposes.<sup>4–7</sup>

In spite of these developments, relatively little effort has been dedicated to elucidating the underlying thermodynamic behavior of scCO<sub>2</sub> with polymers, particularly in the case of multicomponent mixtures. Melnichenko considered the phase behavior of polymers dissolved in scCO<sub>2</sub> in an attempt to quantify the solvent quality of supercritical fluids.<sup>8</sup> Watkins et

al. and Spontak et al. have explored the influence of supercritical fluid diluents on the location of phase boundaries for several polymer blends and block copolymers, and attempted to quantify the effect of these compressible components as plasticizing agents.<sup>9–14</sup> Efforts have been made to develop an understanding of the relationship between scCO<sub>2</sub> concentration and effective interaction parameters between the constituent polymer chains or blocks. Depending on the miscibility of the neat blend system, the introduction of a supercritical diluent has been shown to improve mixing in blends exhibiting upper critical solution temperature (UCST) behavior, and diminish mixing in lower critical solution temperature (LCST) blends. However these analyses fail to acknowledge the multicomponent nature of these systems. The purpose of this paper is to quantify multicomponent interactions in blends of scCO<sub>2</sub>, styrene-acrylonitrile copolymer (SAN) and deuterated poly(methyl methacrylate) (dPMMA).

**Received:** May 25, 2013

**Revised:** July 3, 2013

**Published:** July 25, 2013

Mixtures of SAN and PMMA (in the absence of  $\text{scCO}_2$ ) have been studied at great length due to the tunable miscibility of the polymers and the exemplary mechanical properties that the blends possess. For copolymers containing 10–30% acrylonitrile by weight, the blends exhibit LCST behavior at experimentally accessible temperatures.<sup>15</sup> Outside of that composition window, the polymers are immiscible. The existence of this limited miscibility has been attributed to the strong repulsion between styrene and acrylonitrile, overwhelming the repulsive interaction that either experiences with PMMA. This phenomenon is often referred to as the “copolymer effect”.

Industrially, SAN is prepared by conventional free radical polymerization (FRP). Polymers obtained by this approach are not suited for fundamental thermodynamic studies because the samples have broad molecular weight distributions. Controlled radical polymerization (CRP) techniques enable the synthesis of samples with narrow molecular weight distributions. Atom transfer radical polymerization (ATRP) is one of the most widely used controlled polymerization methods. However, it has been shown that only low molecular weight SAN copolymers can be prepared by this method and that it requires relatively large quantities of copper catalysts.<sup>16,17</sup> A related synthetic method called activators regenerated by electron transfer atom transfer radical polymerization (ARGET ATRP) requires much lower concentrations of the copper catalyst.<sup>18</sup> The reduced concentration of catalyst suppresses undesired side reactions between growing radicals and copper species, enabling the preparation of high molecular weight SAN copolymers with narrow molecular weight distributions.<sup>19</sup>

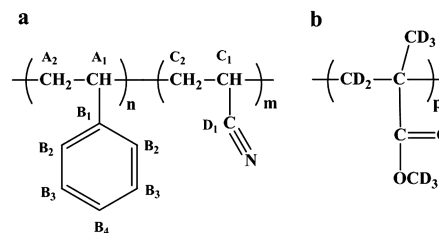
The goal of the work described herein was to use small-angle neutron scattering (SANS) to quantify the thermodynamic interactions in ternary mixtures of  $\text{scCO}_2$ , SAN, and dPMMA. We probed the pairwise interactions of these components using model polymers to allow us to obtain robust thermodynamic parameters. By combining the random phase approximation (RPA) theory for multicomponent mixtures of polymers with information on the solubility of  $\text{scCO}_2$  in SAN and hydrogenous PMMA (hPMMA), we obtained quantitative understanding of the thermodynamics of these multicomponent mixtures, and demonstrated the ability to drastically adjust the limits of the homogeneous phase window.

## 2. EXPERIMENTAL SECTION

**Materials.** Styrene (S, 99.9%), acrylonitrile (AN, >99%), tin(II) 2-ethylhexanoate ( $\text{Sn}(\text{EH})_2$ , 95%), tris[2-(dimethylamino)ethyl]amine ( $\text{Me}_6\text{TREN}$ ), copper(II) chloride ( $\text{CuCl}_2$ , 99.95%), ethyl 2-bromoisobutyrate (EBiB, 98%), anisole (99%), and deuterated chloroform ( $\text{CDCl}_3$ ) were purchased from Sigma-Aldrich.<sup>20</sup> Tetrahydrofuran (THF, 99.9%) and methanol (99.9%) were purchased from Acros, and benzene (99.9%) was purchased from OmniSolv. Both styrene and acrylonitrile monomers were passed through a basic alumina column to remove inhibitors and then purged with argon for 30 minutes. All other chemicals were used as received.

**Synthesis of Styrene–Acrylonitrile Copolymer.** A styrene–acrylonitrile “random” copolymer was synthesized via ARGET ATRP.<sup>19</sup> In reality the SAN copolymer obtained by this approach is a statistical copolymer and we have not characterized sequence distributions in our sample. The chemical structure of SAN is shown in Scheme 1. Styrene (13.3 mL, 116 mmol), acrylonitrile (10 mL, 153 mmol), and anisole (10 mL) were added to a dry Schlenk flask. Argon was bubbled through the Schlenk flask for 15 min. Then the initiator, EBiB (12  $\mu\text{L}$ , 81.7  $\mu\text{mol}$ ) and a solution of  $\text{CuCl}_2$  (0.0074 g, 55  $\mu\text{mol}$ )/ $\text{Me}_6\text{TREN}$  (10  $\mu\text{L}$ , 35.5  $\mu\text{mol}$ ) complex in degassed anisole (5

**Scheme 1.** (a) Styrene–acrylonitrile copolymer structure. Carbon atoms of SAN are labeled for NMR analysis (see text). (b) Deuterated poly(methyl methacrylate) structure.



mL) were added. After stirring the mixture under argon for 10 min, a purged solution of  $\text{Sn}(\text{EH})_2$  (17  $\mu\text{L}$ , 52.4  $\mu\text{mol}$ ) and  $\text{Me}_6\text{TREN}$  (3  $\mu\text{L}$ , 10.6  $\mu\text{mol}$ ) in anisole (5 mL) were added. The sealed flask was placed in thermostated oil bath at 80 °C. Samples were taken at timed intervals and analyzed by gel permeation chromatography (GPC) to follow the progress of the reaction. The polymerization was stopped at the desired number-averaged molecular weight ( $M_n$ ) by opening the flask and diluting with THF. The resulting polymers were isolated from catalyst by passing the reaction mixture through a neutral alumina column and performing two precipitations in methanol. The product was dried under vacuum at 60 °C. The polymers were redissolved at 5 wt % solids in a benzene–THF mixture (90–10% v–v), freeze-dried in a lyophilizer (Millrock LD85), and dried under vacuum at 90 °C for 6 days to remove benzene. <sup>1</sup>H NMR measurements were carried out to determine the weight fraction of acrylonitrile in the SAN copolymer,  $w_{\text{AN}}$ . The obtained copolymer was named following the nomenclature SANXX(yy), where  $\text{XX} = M_n$  in kg/mol and  $\text{yy}$  = the weight percentage of acrylonitrile ( $100 \cdot w_{\text{AN}}$ ).

Commercial SAN copolymer was kindly provided by The Dow Chemical Company. A deuterated PMMA sample (dPMMA125) was purchased from Polymer Source and freeze-dried prior to use.

**Characterization. Gel Permeation Chromatography (GPC).**  $M_n$  and polydispersity index (PDI) were obtained using a Viscotek TDA 302 GPC system that has a guard column, a set of four Viscotek columns (300 mm  $\times$  7.8 mm, T-3000, T-4000, T-5000, and T-6000 columns) and a refractive index detector, with THF eluent (flow rate of 1 mL/min, 35 °C). The instrument was calibrated with polystyrene standards (Agilent Easivials PS-M) and used to quantify  $M_n$  and PDI of materials studied in this manuscript.

**Fourier-Transform Infrared (FT-IR) Spectroscopy.** A Fourier-transform infrared (FT-IR) spectrometer (Thermo Scientific Nicolet 6700), equipped with attenuated total reflection and a germanium crystal, was used to detect the presence of cyano ( $-\text{C}\equiv\text{N}$ ) groups in SAN. Data were collected using OMNIC spectroscopy software.

**Nuclear Magnetic Resonance (NMR) Spectroscopy.** <sup>1</sup>H NMR measurement was conducted on 400 MHz Bruker AVB400 spectrometer using  $\text{CDCl}_3$  solutions with a polymer concentration of  $\sim 5$  mg/mL. <sup>13</sup>C NMR measurement was performed on Bruker BioSpin 900 MHz spectrometer with a polymer concentration of  $\sim 360$  mg/mL at 50 °C for 24 h. Spectra were analyzed to determine copolymer composition.

**Elemental Analysis.** Elemental analysis was carried out using the CHN combustion methodology by Elemental Analysis Incorporated to provide the elemental composition of SAN77(26) in terms of atom weight fraction  $w_i$ , where  $i$  refers to carbon, hydrogen, and nitrogen.

**Blend Film Preparation.** SAN/dPMMA blends were prepared by casting. Predetermined quantities of dPMMA125 and SAN77(26) polymers needed to achieve the desired blend composition were dissolved in THF ( $\sim 0.2$  g/mL) and stirred for 2 days to obtain a homogeneous solution. Films were prepared by slowly drop casting the solution inside O-rings (McMaster Compressible FEP-Encapsulated Silicone O-Rings: nominal thickness = 1/16 in.) to avoid the formation of air bubbles and subsequently dried in ambient atmosphere for 4 days and under vacuum at room temperature for 2 days. The thickness of the films was controlled between 120 and 200  $\mu\text{m}$  by varying the quantity of solution dropped into the O-ring spacer.

We present data from one particular blend which contained 46 volume percent dPMMA. The volume fraction was determined using the density of polymers in the amorphous state,  $T = T_{\text{ref}} = 413$  K and  $P = P_{\text{ref}} = 0.1$  MPa. The density of dPMMA at  $T_{\text{ref}}$  and  $P_{\text{ref}}$  is 1.205 g/cm<sup>3</sup>.<sup>21</sup> The density of SAN copolymer at  $T_{\text{ref}}$  and  $P_{\text{ref}}$  is 1.054 g/cm<sup>3</sup>.<sup>22</sup>

**Differential Scanning Calorimetry (DSC).** DSC experiments were performed on a Thermal Advantage Q200 calorimeter at the Molecular Foundry, Lawrence Berkeley National Laboratory. Samples were sealed in aluminum hermetic pans. DSC scans consisted of two heating/cooling cycles and were conducted over the range 0–150 °C at a rate of 10 °C/min. The glass transition temperatures ( $T_g$ ) for SAN77(26), dPMMA125, and the blend presented in this paper are from the inflection point of the transition in the second heating run.

**Small-Angle Neutron Scattering.** SANS measurements were carried out on the NG3 beamline at the National Institute of Standards and Technology Center for Neutron Research in Gaithersburg, MD. Measurements were first performed at ambient  $P$  ( $P \approx 0.1$  MPa) to quantify the  $T$ -dependent miscibility of the binary polymer blend. For ambient  $P$  experiments, samples were studied at  $T = 60, 100, 120,$  and  $140$  °C by heating in the beamline using a seven-sample  $T$ -control stage, excluding the end positions. Samples were held for at least 30 min at each  $T$  prior to commencing measurements to ensure equilibration. Raw data were corrected for detector sensitivity,<sup>23</sup> background and empty cell scattering contributions, incoherent scattering, and coherent scattering from the pure dPMMA.<sup>24</sup> Data were azimuthally integrated to obtain absolute scattering intensity,  $I$ , as a function of the scattering vector,  $q$ , where  $q = (4\pi/\lambda) \sin(\theta/2)$ ,  $\lambda$  is the incident neutron beam wavelength ( $\lambda = 0.6$  nm), and  $\theta$  is the scattering angle. For ambient  $P$  experiments sample-to-detector distances of 1.33 and 5 m were used, and the data were combined to access the range  $0.133 \text{ nm}^{-1} \leq q \leq 1.838 \text{ nm}^{-1}$ .

Supercritical CO<sub>2</sub> was added to the blend using a modified high- $P$  sample environment provided by NIST. Details of the high- $P$  experiments are provided in the Supporting Information. The sample cell comprised two sapphire windows separated by a 1/16 in. Viton O-ring. Films of the SAN77(26)/dPMMA125 blend were secured within the O-ring and sandwiched between the sapphire windows. This construction was secured within a stainless steel cell housing that could be connected to the scCO<sub>2</sub> source. In this manner, scCO<sub>2</sub> could be introduced to the blend. A digital  $P$ -reader was used to monitor the  $P$  of scCO<sub>2</sub> in contact with the blend. The same sample cell, housing, and  $T$ -control stage were used in the absence and presence of scCO<sub>2</sub>. The blend was thermally equilibrated at the desired  $T$  set point prior to addition of scCO<sub>2</sub> and the sample cell was flushed with CO<sub>2</sub> before pressurization by opening a valve in series with the cell. The valve was then closed and the piston was adjusted to obtain the desired  $P$ . SANS data were obtained using the following protocol: upon reaching the desired  $P$ , a series of three 2 min runs was commenced, followed by a 3 min transmission run. This series of runs was repeated one time, for a total of 12 min of scattering data collection. If time-independent scattering profiles were obtained, the scCO<sub>2</sub> pressure was increased to the next  $P$  and the process was repeated. In some cases, especially near the point of phase separation, the sequence of scattering and transmission runs would be repeated more than twice until equilibrium scattering profiles were obtained or clear evidence of phase separation was observed. All scCO<sub>2</sub> experiments were conducted using a sample-to-detector distance of 5 m, to obtain a  $q$  range of  $0.133 \text{ nm}^{-1} \leq q \leq 0.886 \text{ nm}^{-1}$ . Analysis was performed in an identical manner to that for the ambient pressure experiments.

### 3. THEORETICAL FRAMEWORK

The RPA<sup>25</sup> theory has been used extensively in the past to analyze the coherent scattering intensity,  $I(q)$ , from a homogeneous mixture of polymers, with and without small molecule diluents. The most general form of the expression is given by eq 1:<sup>26</sup>

$$I(q) = \mathbf{B}^T \underline{\underline{S}}(q) \mathbf{B} \quad (1)$$

For our system, the multicomponent structure factor  $\underline{\underline{S}}(q)$  is a 2 by 2 matrix with elements  $S_{ij}$  that describe the correlations between components  $i$  and  $j$ . scCO<sub>2</sub>, SAN, and dPMMA are referred to as components 1, 2, and 3, respectively. Elements of the column vector  $\mathbf{B}$ , which quantifies the scattering contrast between components, are:

$$B_i = \frac{b_i}{v_i} - \frac{b_3}{v_3} \quad (i = 1, 2) \quad (2)$$

where  $b_i$  and  $v_i$  are the scattering length and the monomer volume of component  $i$ , respectively. The dependence of  $b_i/v_i$  on  $P$  for each pure component is included in the Supporting Information (Figure S1). Equation 3 provides the definition of matrix  $\underline{\underline{S}}(q)$ , illustrating the additive contributions of correlations in the absence and presence of interactions:

$$\underline{\underline{S}}(q) = [\underline{\underline{S}}^\circ(q)^{-1} + \underline{\underline{V}}(q)]^{-1} \quad (3)$$

The ideal structure factor matrix,  $\underline{\underline{S}}^\circ(q)$ , contains information on the correlations between components in the absence of thermodynamic interactions. The matrix consists of the following elements:

$$S_{ii}^\circ(q) = N_i \phi_i v_i P_i(q) \quad (i = 1, 2) \quad (4)$$

$$S_{ij}^\circ(q) = 0 \quad (i \neq j) \quad (5)$$

The average number of monomer units in a chain is  $N_i$  ( $N_i = M_{w,i}/M_{0,i}$  where  $M_{0,i}$  is the monomer molecular weight) and  $\phi_i$  is the volume fraction of component  $i$  in the blend. We ignore the heterogeneous nature of SAN chains and assume that  $v_2$  is the volume-weighted average of the styrene and acrylonitrile monomer volumes, which we take to be 0.179 nm<sup>3</sup> and 0.0819 nm<sup>3</sup> at 413 K, respectively, as calculated from the mass densities;  $v_2 = 0.156 \text{ nm}^3$ . The mass-weighted average of styrene and acrylonitrile monomer molecular weight is  $M_{0,2}$  ( $M_{0,2} = 90.9$  g/mol). Correlations between monomers along a given chain are represented by the partial structure factor  $S_{ii}^\circ(q)$ , which is based on the single-component form factor for each component of the mixture as given by the Debye function for flexible chains:

$$P_i(q) = \frac{2}{u_i^2} [\exp(-u_i) + u_i - 1] \quad (6)$$

where  $u_i = q^2 R_{g,i}^2$  and  $R_{g,i}^2 = N_i l_i^2 / 6$ .  $R_{g,i}$  is the radius of gyration for a chain of species  $i$ , and  $l_i$  is the statistical segment length.  $N_1$  is taken to be unity, and  $P_1(q) = 1$  at all values of  $q$  due to the lack of connectivity between the scCO<sub>2</sub> molecules. The statistical segment length of dPMMA ( $l_3$ ) is 0.54 nm at  $T_{\text{ref}} = 413$  K,<sup>21</sup> while that of SAN ( $l_2$ ) is determined as described subsequently in this work. The interaction matrix  $\underline{\underline{V}}(q)$  is given by

$$V_{ii}(q) = \frac{1}{N_3 \phi_3 v_3 P_3(q)} - \frac{2\chi_{i3}}{v_0} \quad (i = 1, 2) \quad (7)$$

$$V_{ij}(q) = \frac{1}{N_3 \phi_3 v_3 P_3(q)} - \frac{\chi_{i3}}{v_0} - \frac{\chi_{j3}}{v_0} + \frac{\chi_{ij}}{v_0} \quad (i \neq j) \quad (8)$$

The Flory–Huggins interaction parameter,  $\chi_{ij}$ , quantifies the interactions between species  $i$  and  $j$ , and  $v_0$  is an arbitrary reference volume. In this work,  $v_0$  is set equal to 0.1 nm<sup>3</sup>. Equations 1–8 are derived on the assumption that  $\delta\phi_1(\mathbf{r}) + \delta\phi_2(\mathbf{r}) + \delta\phi_3(\mathbf{r}) = 0$  at each  $T$  and  $P$  ( $\mathbf{r}$  is an arbitrary position

in the blend and  $\delta\phi_i(\mathbf{r})$  is the local fluctuation in the volume fraction of component  $i$  at  $\mathbf{r}$ . RPA expressions derived under this assumption are sometimes called “incompressible” RPA. We believe that the use of the term “incompressible” is inappropriate. In the literature, it is routine to employ this assumption in analysis of SANS data at atmospheric pressure. In ref 27, it has been argued that the validity of this assumption increases with increasing pressure. We use RPA expressions to analyze our data regardless of  $T$  and  $P$ . The  $T$  and  $P$  values in this paper are well-removed from the critical point of  $\text{CO}_2$ . It is expected that the theory will break down near the critical point of  $\text{CO}_2$  due to the dominance of density fluctuations. SANS profiles as a function of  $T$  and  $P$  from single-phase binary (SAN and dPMMA) and multicomponent ( $\text{scCO}_2$ , SAN, and dPMMA) mixtures were used to obtain  $\chi_{ij}$  and  $l_i$  by performing nonlinear least-squares fits of the RPA expression (eqs 1–8). Rather than fitting the data by varying  $l_2$  and  $l_3$  independently, a multiplicative constant  $\alpha$  is used to adjust both simultaneously:<sup>27,28</sup>

$$l_i(T, P) = \alpha_i(T, P)l_{i,\text{ref}} \quad (i = 2, 3) \quad (9)$$

Here,  $l_{i,\text{ref}}$  is the statistical segment length of species  $i$  at  $T_{\text{ref}}$  and  $P_{\text{ref}}$ . Thus,  $\alpha$  can be considered an average expansion factor for SAN and dPMMA which quantifies the effect of  $T$  and  $P$  on chain configuration.

Combining eqs 1–8 yields the primary result of this section, the expression for  $I(q)$  for the multicomponent mixtures of interest:

$$I(q) = B_1^2 S_{11}(q) + 2B_1 B_2 S_{12}(q) + B_2^2 S_{22}(q) \quad (10)$$

$$S_{11}(q) = \frac{\frac{1}{S_{22}^{\circ}} + V_{22}}{\left(\frac{1}{S_{11}^{\circ}} + V_{11}\right)\left(\frac{1}{S_{22}^{\circ}} + V_{22}\right) - V_{12}^2} \quad (11)$$

$$S_{22}(q) = \frac{\frac{1}{S_{11}^{\circ}} + V_{11}}{\left(\frac{1}{S_{11}^{\circ}} + V_{11}\right)\left(\frac{1}{S_{22}^{\circ}} + V_{22}\right) - V_{12}^2} \quad (12)$$

$$S_{12}(q) = \frac{-V_{12}}{\left(\frac{1}{S_{11}^{\circ}} + V_{11}\right)\left(\frac{1}{S_{22}^{\circ}} + V_{22}\right) - V_{12}^2} \quad (13)$$

It is implicit in eqs 1–8 that the free energy of mixing per unit volume ( $\Delta G_m$ ) for a mixture of a diluent (component 1) and two polymers (components 2 and 3) is given by the Flory–Huggins Theory:<sup>29,30</sup>

$$\begin{aligned} \frac{\Delta G_m}{kT} = & \frac{\phi_1 \ln \phi_1}{v_1} + \frac{\phi_2 \ln \phi_2}{v_2 N_2} + \frac{\phi_3 \ln \phi_3}{v_3 N_3} + \frac{\chi_{12} \phi_1 \phi_2}{v_0} \\ & + \frac{\chi_{13} \phi_1 \phi_3}{v_0} + \frac{\chi_{23} \phi_2 \phi_3}{v_0} \end{aligned} \quad (14)$$

Expressions for  $\Delta G_m$  for a  $\text{scCO}_2$ /polymer mixture can be obtained from eq 14 setting either  $\phi_2$  or  $\phi_3 = 0$ . The expression thus obtained is:

$$\begin{aligned} \frac{\Delta G_{m,1-i}}{kT} = & \frac{\phi_{1-i} \ln \phi_{1-i}}{v_1} + \frac{(1 - \phi_{1-i}) \ln(1 - \phi_{1-i})}{v_i N_i} \\ & + \frac{\chi_{1i} \phi_{1-i} (1 - \phi_{1-i})}{v_0} \end{aligned} \quad (15)$$

The subscript  $1-i$  refers to either of the two  $\text{scCO}_2$ -polymer binary mixtures, and  $\phi_{1-i}$  is the volume fraction of  $\text{scCO}_2$  in the binary mixture. The chemical potential of  $\text{scCO}_2$ ,  $\mu_{1-i}$ , in these binary mixtures is given by:

$$\begin{aligned} \frac{\Delta \mu_{1-i}}{RT} = & \chi_{1i} (1 - \phi_{1-i})^2 + \frac{v_0}{v_1} \ln(\phi_{1-i}) \\ & + (1 - \phi_{1-i}) \left( \frac{v_0}{v_1} - \frac{v_0}{v_i N_i} \right) \end{aligned} \quad (16)$$

$\Delta \mu_{1-i}$  is defined as the difference between  $\mu_{1-i}(T, P)$  and  $\mu_{1-i}^{\circ}(T, P)$ , where  $\mu_{1-i}^{\circ}(T, P)$  is the chemical potential of the pure  $\text{CO}_2$  at the  $T$  and  $P$  of interest, and  $R$  is the ideal gas constant.

In the limit  $\phi_1 \rightarrow 0$ , eqs 10–13 reduce to the standard RPA expression for binary polymer blends:

$$I(q) = I_{\text{bin}}(q) = \left( \frac{b_2}{v_2} - \frac{b_3}{v_3} \right)^2 \left( \frac{1}{S_{22}^{\circ}(q)} + \frac{1}{S_{33}^{\circ}(q)} - \frac{2\chi_{23}}{v_0} \right) \quad (17)$$

and  $\Delta G_m$  is given by:

$$\begin{aligned} \frac{\Delta G_m}{kT} = & \frac{\phi_3 \ln \phi_3}{v_3 N_3} + \frac{(1 - \phi_3) \ln(1 - \phi_3)}{v_2 N_2} \\ & + \frac{\chi_{23} \phi_3 (1 - \phi_3)}{v_0} \end{aligned} \quad (18)$$

The Flory–Huggins estimate of the critical volume fraction for the blend can be derived from eq 18, assuming that  $\chi_{23}$  is only a function of  $T$ :

$$\phi_{3,\text{crit}} = \frac{1}{1 + (N_3^*/N_2^*)^{1/2}} \quad (19)$$

Here we use a modified definition of chain length where  $N_i^*$  is defined as the number of repeat units of volume  $v_0$ :  $N_i^* = N_i v_i / v_0$ . For a binary symmetric blend with  $N_2^* = N_3^* = N^*$ , the critical point is given by  $\chi N^* = 2$ . For an asymmetric blend with  $N_2^* \neq N_3^*$  the critical point is given by  $\chi N_{\text{AVE}}^* = 2$ , where  $N_{\text{AVE}}^*$ :

$$N_{\text{AVE}}^* = 4 \left[ \frac{1}{(N_2^*)^{1/2}} + \frac{1}{(N_3^*)^{1/2}} \right]^{-2} \quad (20)$$

Equations 10–13 are used to analyze  $\text{scCO}_2$ /SAN/PMMA mixtures, eq 16 is used to analyze  $\text{scCO}_2$ /SAN and  $\text{scCO}_2$ /PMMA mixtures, and eqs 17–20 are used to analyze SAN/PMMA mixtures.

## 4. RESULTS AND DISCUSSION

**SAN Copolymer Characterization.** Figure 1 shows the GPC traces of SAN synthesized by ARGET ATRP (SAN77(26),  $M_n = 77$  kg/mol,  $M_w = 100$  kg/mol, PDI = 1.30) and the commercial SAN sample (SAN44(18),  $M_n = 44$  kg/mol,  $M_w = 104$  kg/mol, PDI = 2.34). It is evident in Figure 1 that the sample synthesized by ARGET ATRP has a significantly narrower molecular weight distribution than the commercial sample.

FT-IR spectra of SAN77(26) and SAN44(18) are shown in Figure 2. A spectrum obtained from the polystyrene homopolymer PS48 is also shown as a reference. Both SAN77(26) and SAN44(18) have a clear absorption peak at approximately  $2236 \text{ cm}^{-1}$  indicating the presence of cyano

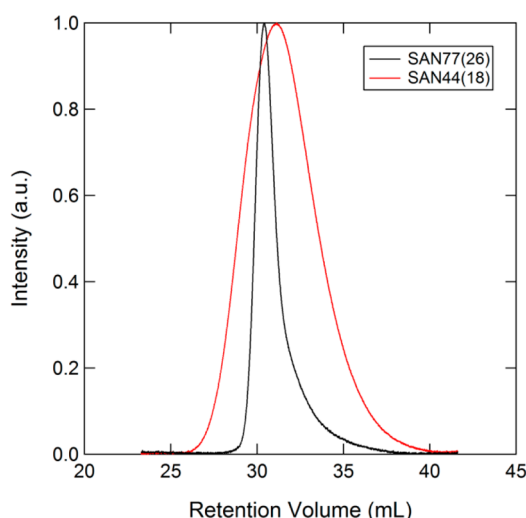


**Figure 1.** GPC traces comparing  $M_n$  and PDI of SAN77(26) (black solid line), prepared in this work by ARGET ATRP, with a commercially available SAN copolymer, SAN44(18) (red solid line), synthesized by FRP.

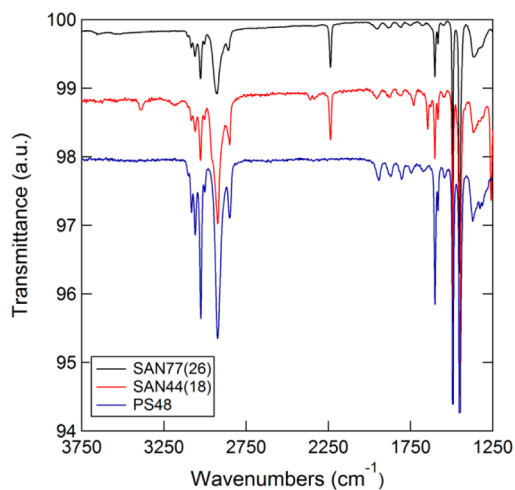


**Figure 2.** FT-IR spectra showing  $-C\equiv N$  stretching absorption signatures ( $2236\text{ cm}^{-1}$ ) to indicate presence of acrylonitrile in SAN77(26) (black solid line), synthesized by ARGET ATRP, as well as SAN44(18) (red solid line), synthesized by FRP. Homopolymer PS48 (blue solid line) has no absorption in the relevant wavenumber range. The spectra are shifted vertically for clarity.

groups.<sup>31</sup> In contrast, the spectrum of PS48 is featureless in the range  $2800$  to  $2000\text{ cm}^{-1}$ .

Three methods were used to quantify the SAN copolymer composition:  $^1\text{H}$  NMR,  $^{13}\text{C}$  NMR, and elemental analysis. Distinguishing between SAN77(26) and PS48 using  $^1\text{H}$  NMR is difficult. The unique chemical shifts of the acrylonitrile groups overlap with those of the hydrocarbon backbone of PS. One estimate of the copolymer composition was found by comparing the area of all backbone peaks ( $0.5$ – $3.0\text{ ppm}$ ) with that of the aromatic peak area ( $6.4$ – $7.4\text{ ppm}$ ). By this methodology, the copolymer is estimated to have  $w_{\text{AN}} = 0.26$ .

$^{13}\text{C}$  NMR spectroscopy was used to obtain unique signatures of styrene and acrylonitrile groups in SAN.<sup>32</sup> The aromatic carbon atoms forming the phenyl group of styrene have  $^{13}\text{C}$  NMR chemical shifts between  $120$  and  $150\text{ ppm}$ , while the

nitrile carbon has a chemical shift differing from the aromatic peaks (peak D1). Finally, the backbone carbon atoms have shifts in the  $20$ – $60\text{ ppm}$  range. In Scheme 1, the carbon atoms of SAN are labeled as Yz, where Y refers to the group of related carbon atoms and z represents our numbering scheme. Figure 3 shows the  $^{13}\text{C}$  NMR spectrum of SAN77(26), with peaks labeled according to nomenclature of Scheme 1. By this methodology, the copolymer is estimated to have  $w_{\text{AN}} = 0.25$ .

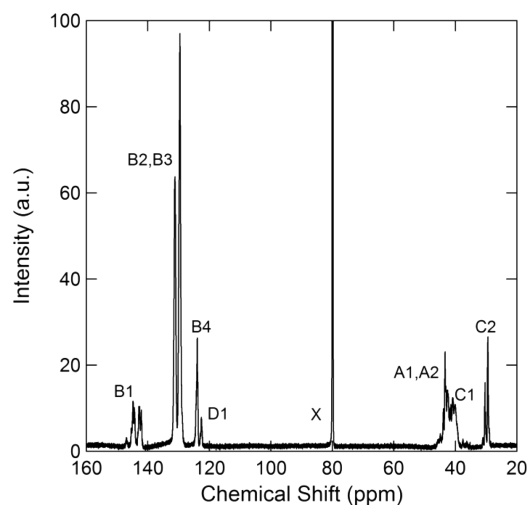


**Figure 3.**  $^{13}\text{C}$  NMR spectrum of SAN77(26). The peaks assignments are based on the structure of SAN shown in Scheme 1. The peak areas are used in conjunction with the known carbon group ratios to determine the copolymer composition. The peak marked X represents the chemical shift associated with the solvent, deuterated chloroform.

Elemental analysis using standard combustion procedures yielded the weight fractions of carbon, hydrogen, and nitrogen:  $w_{\text{C}} = 0.85$ ,  $w_{\text{H}} = 0.071$ , and  $w_{\text{N}} = 0.073$ . By this methodology, the copolymer is estimated to have  $w_{\text{AN}} = 0.28$ .

The characteristics of SAN77(26) and dPMMA125 are summarized in Table 1, where we report the  $M_n$ ,  $M_w$ , PDI,  $w_{\text{AN}}$ , and  $N$  for the copolymer. dPMMA125 was only characterized by GPC, to measure  $M_n$ ,  $M_w$ , PDI, and  $N$ .

Table 2 provides an overview of the results of DSC experiments on SAN77(26), dPMMA125, and the blend. The  $T_g$  of a homogeneous blend can be estimated using the Fox equation:

$$\frac{1}{T_{g,\text{blend}}} = \frac{w_2}{T_{g,2}} + \frac{w_3}{T_{g,3}} \quad (21)$$

In eq 21,  $T_{g,i}$  and  $w_i$  refer to the  $T_g$  and weight fraction of each component in the blend. The predicted  $T_g$  of the blend using eq 21 is  $(393 \pm 4)\text{ K}$ , which is consistent with the value reported in Table 2.

The blend studied in this work was designed such that the composition of the undiluted blend,  $\phi_3$ , was close to the critical composition, as defined in eq 19:  $\phi_3 \approx \phi_{3,\text{crit}} = 0.493$ . Using eq 20, we obtain  $N_{\text{AVE}}^* = 1764$ .

**Binary  $\text{scCO}_2$ –Polymer Blend.** The solubility of  $\text{scCO}_2$  in SAN and PMMA at  $313\text{ K}$  is quantified in Figure 4a, where the weight fraction of  $\text{scCO}_2$  in each polymer,  $w_{1,i}$ , is given as a function of  $P$ . The data in Figure 4a were provided to us by scientists at The Dow Chemical Company.<sup>33</sup> The measurements were made on commercial polymers with similar  $M_w$  and copolymer composition (in the case of SAN) to those used in

Table 1. Polymer Characteristics

polymer	$M_n$ (kg/mol)	$M_w$ (kg/mol)	PDI	composition ( $w_{AN}$ )			
				$^1\text{H}$ NMR	$^{13}\text{C}$ NMR	elem. anal.	$N$
SAN77(26)	77	100	1.30	26	25	28	1202
dPMMA125	125	131	1.05	–	–	–	1218

Table 2. Thermal Characterization of Blend and Constituent Polymers by DSC

sample	$T_g$ (K)
SAN77(26)	$386 \pm 2$
dPMMA125	$399 \pm 4$
blend	$388 \pm 3$

this work. (Scientists at Dow indicated that the solubilities of  $\text{scCO}_2$  in SAN and PMMA are independent of  $M_w$ , PDI, and deuteration. Our analysis is based on this simplification.)

At a given  $T$  and  $P$ ,  $\text{scCO}_2$ /SAN and  $\text{scCO}_2$ /PMMA mixtures with  $\text{scCO}_2$  weight fractions  $w_{1-2}$  and  $w_{1-3}$ , respectively, are in thermodynamic equilibrium with  $\text{scCO}_2$  at the same  $T$  and  $P$ . Thus, the chemical potential of  $\text{scCO}_2$  in the two mixtures  $\mu_{1-i}$  must be equal. We use Flory–Huggins Theory (eq 15) to derive an expression that relates  $\chi_{12}$  to  $\chi_{13}$  based on this equality:

$$\chi_{12} = \frac{1}{(1 - \phi_{1-2})^2} \left[ \chi_{13} (1 - \phi_{1-3})^2 + \frac{v_0}{v_1} \ln \frac{\phi_{1-3}}{\phi_{1-2}} + (1 - \phi_{1-3}) \left( \frac{v_0}{v_1} - \frac{v_0}{N_3 v_3} \right) - (1 - \phi_{1-2}) \left( \frac{v_0}{v_1} - \frac{v_0}{N_2 v_2} \right) \right] \quad (22)$$

where  $\phi_{1-i}$  are obtained from  $w_{1-i}$  using the previously given  $v_i(T, P)$  for the polymers and  $v_1$  varies with  $P$  as seen in Figure 4b.<sup>34</sup>

It is evident from eq 22 that  $\chi_{12}$  at a given value of  $T$  and  $P$  is constrained to be a linear function of  $\chi_{13}$  (that is,  $\chi_{12} = A_1 \chi_{13} + A_2$ , where  $A_1$  and  $A_2$  are constants at each  $T$  and  $P$ ). Figure 4c shows this function at 313 K at the lowest and highest values of  $P$  considered in this work, and all of the coefficients relevant to this study are summarized in Table 3.

**Binary Polymer Blend.** Small-angle neutron scattering profiles obtained from a blend of SAN77(26) and dPMMA125 with  $\phi_3 = 0.461$  at atmospheric  $P$  (in the absence of  $\text{scCO}_2$ ) are shown in Figure 5, where  $I(q)$  vs  $q$  is presented as a function of  $T$ . Over the entire  $T$  range studied, the scattering profiles have the shape expected for homogeneous polymer blends, with a plateau at low  $q$ . The 333 K data were acquired using the high- $P$  configuration with a narrower  $q$  window. The low  $q$  intensity increases with increasing  $T$ . This indicates that the miscibility decreases with increasing  $T$ . The solid lines in Figure 5 are fits of binary polymer blend RPA (eq 17). It is evident that the SANS profiles are in quantitative agreement with binary RPA. The 413 K data were fit with  $\chi_{23}$  and  $l_2$  as adjustable parameters (we were unable to find the statistical segment length of SAN77(26) in the literature). We assume that  $l_3 = 0.54$  nm at  $T = 413$  K and  $P = 0.1$  MPa.<sup>21</sup> The value of  $l_2$  thus obtained was 0.83 nm. The 373 and 393 K data were fit with  $\chi_{23}$  and  $\alpha$  as fitting parameters. The fitted value of  $\alpha$  at these temperatures was found to be  $0.997 \pm 0.005$ . This implies that chain

configurations are not affected by  $T$  in this regime. The values of  $\chi_{23}$  obtained in the 373–413 K range are shown by filled symbols in Figure 6. We use the usual empirical function to describe the  $T$ -dependence of  $\chi_{23}$

$$\chi = C + \frac{D}{T} \quad (23)$$

where  $C$  and  $D$  are fitting parameters. A least-squares fit gives the line in Figure 6,  $\chi_{23} = 0.0920 - 39.622/T$ . The dashed line in Figure 6 is an extrapolation of eq 23 to  $T = 333$  K. The empty circle in Figure 6 shows  $\chi_{23}$  obtained from the SANS fit at this value of  $T$ . Note that  $T_g$  of the blend (388 K) is substantially higher than 333 K. We thus expect that this sample was not well-equilibrated. In spite of this, we find that extrapolations of  $\chi_{23}$  based on data obtained at higher temperatures are not too different from the explicit measurement at 333 K. The value of  $\alpha$  obtained at  $T = 333$  K was 1.27. It thus appears that the main effect of the departure from equilibrium is coil expansion, where the chains are kinetically trapped in a swollen state during sample preparation. Our analysis of the binary data ignores the possibility that the data at 373 K may be affected by nonequilibrium effects as  $T_g$  of the blend is slightly higher.

The SANS data is presented in the form of a Zimm plot in Figure 7a, using the truncated range  $0.133 \text{ nm}^{-1} < q < 0.250 \text{ nm}^{-1}$ . It is evident that the data can be fit with reasonable success to linear expressions, as represented by solid lines in Figure 7a. Extrapolation of these fits to  $q = 0 \text{ nm}^{-1}$  yields values of  $I_{0,\text{Zimm}}$  over the  $T$  range studied. In addition, the RPA fits to the data were extrapolated to  $q = 0$  to obtain  $I(q = 0) = I_{0,\text{RPA}}$ . In Figure 7b, we plot both  $1/I_{0,\text{Zimm}}$  and  $1/I_{0,\text{RPA}}$  versus  $1/T$ . It is evident that both  $1/I_{0,\text{Zimm}}$  and  $1/I_{0,\text{RPA}}$  are linear functions of  $1/T$ . (The 333 K data showed as unfilled symbols in Figure 7b were not included in the fit.) Estimates of the blend phase separation  $T$  ( $T_s$ ) are obtained by extrapolating the lines in Figure 7b to meet the abscissa. The Zimm analysis predicts  $T_s = (440 \pm 10)$  K, while the RPA analysis predicts  $T_s = (430 \pm 30)$  K. These values are in reasonable agreement with each other, providing an estimated value of  $T_s = (430 \pm 40)$  K. Concerns about polymer degradation prevented us from conducting experiments near  $T_s$ .

**Multicomponent Blend.** Figure 8 shows  $I(q)$  obtained from a blend of  $\text{scCO}_2$ /SAN77(26)/dPMMA125 with  $\phi_{3,0} = 0.461$  (i.e., in the absence of  $\text{scCO}_2$ ) at  $T = 313$  K as a function of  $P$  in the range  $9.7 \text{ MPa} \leq P \leq 27.6 \text{ MPa}$ . The scattering profiles are qualitatively similar to the binary scattering profiles shown in Figure 5. It is evident that the low  $q$  plateau obtained in the multicomponent blends increases with increasing  $P$ . This indicates approach toward macrophase separation with increasing  $P$ . The SANS profiles obtained at  $P = 31$  MPa were strong functions of time, and qualitatively different from the profiles shown in Figure 8.

We used the multicomponent RPA to analyze the SANS data shown in Figure 8. We assume that  $\text{scCO}_2$  plasticizes our blend and facilitates equilibration. This effect has been demonstrated previously where the presence of  $\text{scCO}_2$ , even in the case where it does not behave as a good solvent, has been shown to decrease

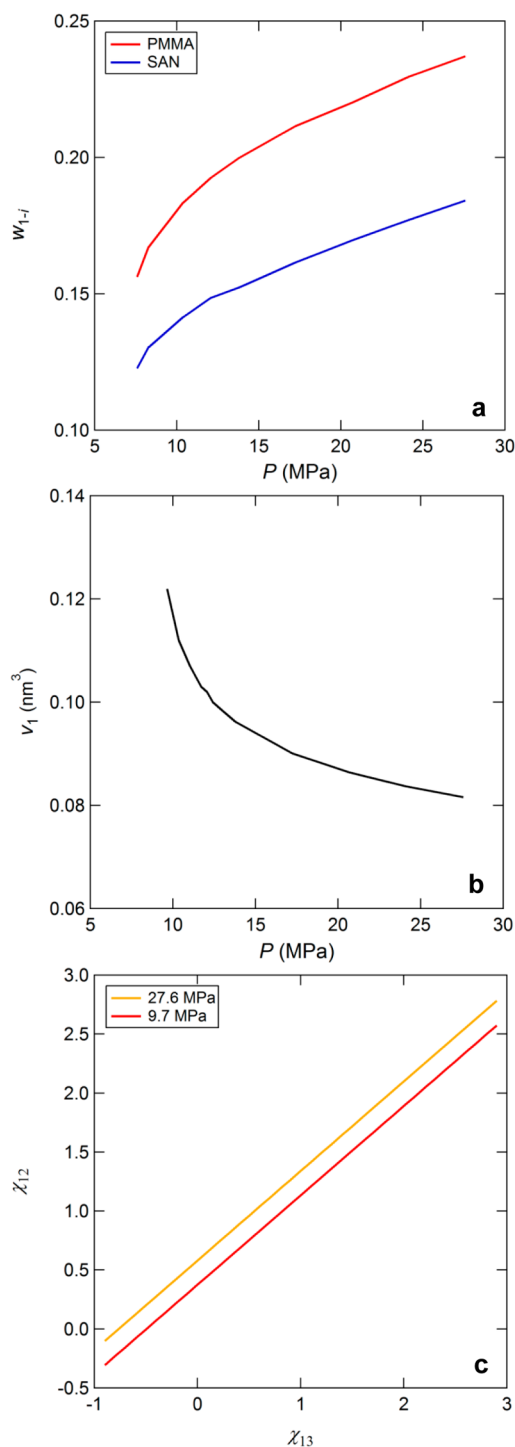


**Figure 4.** (a) Carbon dioxide (component 1) solubility in SAN copolymer ( $w_{AN} = 0.26$ ) (component 2) and hydrogenous poly(methyl methacrylate) (component 3), expressed as  $w_{1-i}$  the weight fraction of  $\text{scCO}_2$  in pure polymer  $i$ , as a function of  $P$ , in the supercritical regime ( $T = 313 \text{ K}$  and  $P > P_{c,\text{CO}_2}$ ). (b) The molecular volume of  $\text{scCO}_2$  varies monotonically with  $P$  across the  $P$ -range of interest at  $313 \text{ K}$ . (c) Linear relationship between  $\chi_{12}$  to  $\chi_{13}$  obtained from equating chemical potential of  $\text{scCO}_2$  in the binary blends. The red line shows the relationship for the lowest  $P$  studied in this work,  $9.7 \text{ MPa}$ , while the orange line shows the relationship for the highest  $P$  studied for which a homogeneous mixture was obtained ( $27.6 \text{ MPa}$ ).

the  $T_g$  of polymers dramatically.<sup>35</sup> The solid curves represent multicomponent RPA fits using eq 11 with two adjustable

**Table 3.** Pressure-Dependent Coefficients for Relationship Between  $\chi_{12}$  and  $\chi_{13}$

$P$ (MPa)	$A_1$	$A_2$
9.7	0.757	0.376
12.4	0.768	0.472
17.2	0.763	0.539
20.7	0.764	0.554
24.1	0.760	0.581
27.6	0.759	0.586

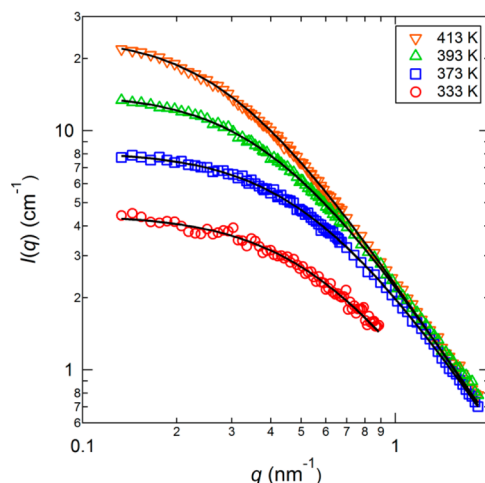


**Figure 5.** Small-angle neutron scattering results from a blend of deuterated poly(methyl methacrylate), dPMMA125, and styrene-acrylonitrile random copolymer, SAN77(26), studied as a function of  $T$ . The blend contained 46.1% dPMMA125 by volume. The scattering experiments were performed at  $333 \text{ K}$  (red circles),  $373 \text{ K}$  (blue squares),  $393 \text{ K}$  (green triangles), and  $413 \text{ K}$  (orange inverted triangles). The solid lines are binary random phase approximation fits to the data with the Flory–Huggins interaction parameter,  $\chi_{23}$ , and  $\alpha$ , the average expansion factor, as adjustable parameters. Error bars on the SANS data points representing one standard deviation in the measured intensity are within the size of the data symbols.

parameters:  $\chi_{13}$  and  $\alpha$ . All other parameters required to calculate  $I(q)$  were determined *a priori*.  $\phi_1$  was estimated using the solubility data shown in Figure 4a. If we assume the volume change of mixing is negligible, then the total  $\text{scCO}_2$  volume fraction can be calculated directly using the binary solubility data ( $w_{1-i}$ ) along with the pure component monomer and molecular volumes. The dependence of  $\phi_1$  on  $P$  thus obtained is shown in Figure 9a. At  $P < 10 \text{ MPa}$ , the change in  $\phi_1$  is dominated by changes in the molar volume of  $\text{scCO}_2$  in the vicinity of the critical point of  $\text{CO}_2$ . Increasing  $P$  in this regime results in a sharp reduction of  $\phi_1$ . In contrast, a gradual increase in  $\phi_1$  is seen at  $P > 10 \text{ MPa}$  due to the increased solubility of  $\text{scCO}_2$  in both polymers.

The value of  $\chi_{23}$  is obtained by extrapolating eq 20 to  $313 \text{ K}$ . On the basis of previous work,<sup>27,28,36</sup> we expect polymer–polymer interactions to be unaffected by changes in hydrostatic  $P$  in the range  $9.7 \text{ MPa} \leq P \leq 27.6 \text{ MPa}$ . Consequently, a constant value of  $\chi_{23} = -0.0346$  was used for all  $P$ .

We have thus determined all of the parameters needed to calculate  $I(q)$  (eqs 11–14) of our blend, except  $\chi_{12}$  and  $\chi_{13}$ . However these two parameters are not independent and the relationship between them is given in Figure 4c and Table 3. In Figure 10 we plot  $I_{0,\text{RPA}}$  calculated using eqs 11–14 as a function of  $\chi_{13}$  at  $T = 313 \text{ K}$  and  $P = 9.7 \text{ MPa}$ . For each value of  $\chi_{13}$ , a

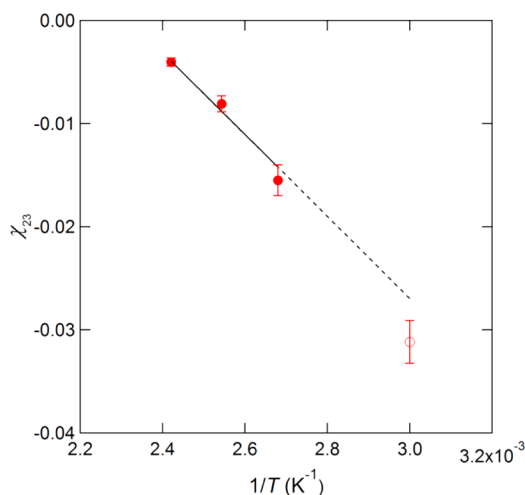


**Figure 6.** Flory–Huggins interaction parameter between SAN77(26) and dPMMA125,  $\chi_{23}$ , as a function of  $1/T$  obtained from random phase approximation fits for a blend containing 46.1% dPMMA125 by volume. The data is fit by least-squared linear regression over the range of  $T \geq 373$  K to obtain the expression  $\chi_{23} = 0.0920 - 39.622/T$ , shown as solid black line. The dashed line is the extrapolation of  $\chi_{23}(T)$  to 333 K, to illustrate that the data collected at that  $T$  is close to high  $T$  extrapolation, despite being well below  $T_g$ .

corresponding value of  $\chi_{12}$  was calculated according to eq 19. The range of  $\chi_{13}$  is restricted to include positive  $I_{0,RPA}$  values only. It is clear that  $I_{0,RPA}$  is a nonmonotonic function of  $\chi_{13}$  and that  $I_{0,RPA}$  diverges as  $\chi_{13}$  approaches both  $-0.9$  and  $1.52$ . The horizontal line in Figure 10 represents the value of  $I_0$  obtained from the experiments using the Zimm extrapolation. This line intersects the  $I_{0,RPA}$  vs  $\chi_{13}$  curve at two points:  $\chi_{13} = 0.269$  and  $\chi_{13} = 1.499$ . Both of these values of  $\chi_{13}$  produce RPA curves that are consistent with the SANS profiles. We eliminate the value of  $\chi_{13} = 0.269$  on physical grounds; we know that  $scCO_2$  is not a good solvent for dPMMA. We thus conclude that  $\chi_{13}$  is  $1.499$ , and eq 19 gives  $\chi_{12} = 1.512$ .

The procedure described in the previous paragraph was repeated at all  $P$  of interest, and the resulting values of  $\chi_{12}$  and  $\chi_{13}$  thus obtained are shown in Figure 11. To a good approximation,  $\chi_{12}$  is equal to  $\chi_{13}$ . We propose the following empirical function for describing the dependence of  $\chi_{12}$  and  $\chi_{13}$  on  $P$ :

$$\chi_{13} = 2.503 - \frac{3.038}{P - 6.626} \quad (24)$$

This completes determination of all parameters required to compute  $I(q)$ . The solid curves in Figure 8 show the results of our analysis. It is perhaps remarkable that a mean-field theory such as multicomponent RPA can be used to describe SANS data from mixtures as complex as  $scCO_2$ /SAN/dPMMA. It is evident that as  $P$  increases the agreement between the scattering profiles and the multicomponent RPA becomes less quantitative. Considering the 13 parameters needed to describe the scattering (11 of which are measured from independent experiments), it is not clear as of now which would allow an improvement in the agreement between experiment and theory. The values of  $\alpha$  obtained from our analysis are  $1.47 \pm 0.09$  with all values within 9% of the average. This implies that the chain dimensions in the presence of  $scCO_2$  of our polymers are about 47% larger than that obtained in the rubbery blend without  $scCO_2$ . It is worth noting that the two main parameters that

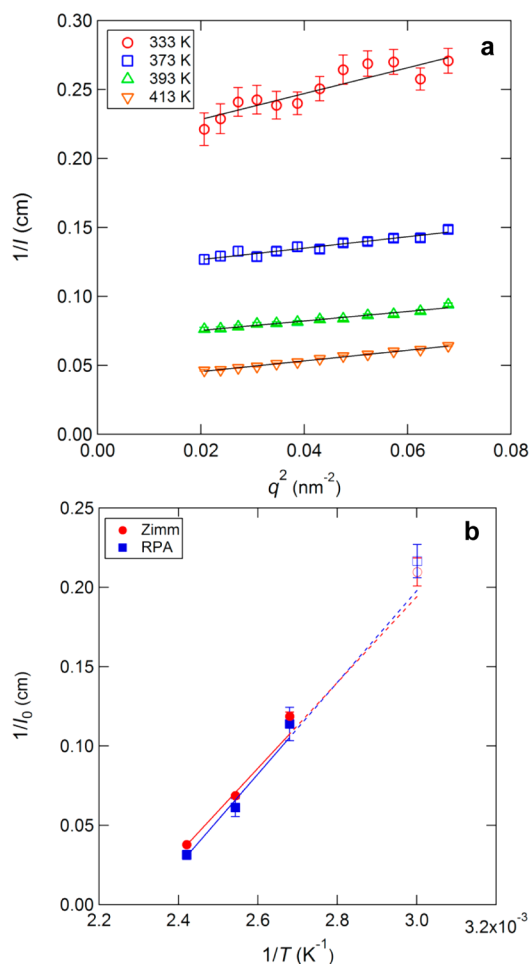


**Figure 7.** (a) Reciprocal of the absolute scattering intensity,  $1/I$ , plotted against  $q^2$ , for a blend containing 46.1% dPMMA125 by volume as a function of  $T$  at ambient  $P$ . The scattering experiments were performed at 333 K (red circles), 373 K (blue squares), 393 K (green triangles), and 413 K (orange inverted triangles). Least-squared linear fits to the data are shown with solid lines. (b) Comparison of the plots of  $1/I_0$  versus  $1/T$ , obtained from Zimm plots (red circles) and RPA (blue squares),  $I_0$  is the SANS intensity as  $q$  approaches  $0 \text{ nm}^{-1}$ . The data is fit with a least-squares linear regression to find  $T$  at which  $I_0$  diverges (i.e.,  $1/I_0 = 0$ ). This provides an estimate of the phase separation temperature,  $T_s$ ;  $T_s = 440$  K for the Zimm method and  $T_s = 430$  K for the RPA method. Open symbols represents experiments performed at  $T = 333$  K (not included in the fit).

govern the thermodynamics of the mixture are  $\chi_{13}$  (or  $\chi_{12}$  since they are nearly equal) and  $\chi_{23}$  are simple functions of  $P$  ( $\chi_{23}$  is independent of  $P$ ). The parameters that display complex nonmonotonic  $P$ -dependencies are  $\phi_1$  and  $\nu_1$  (Figure 4b and Figure 9a, respectively). The values of  $\chi_{13}$  presented here (eq 24) can be examined in the context of previously reported values for dPMMA- $scCO_2$ ; for example Koga et al.<sup>38</sup> report that at 11.25 MPa and 309 K,  $\chi_{13} = 0.993$ , while our work indicates that at the same  $P$  and 313 K,  $\chi_{13} = 1.846$ . Koga et al. use a constant molar volume for  $CO_2$  of  $46 \text{ cm}^3/\text{mol}$  to calculate the reference volume ( $\nu_1 = 0.0764 \text{ nm}^3$ ), so their reported value of  $\chi_{13}$  (1.30) is scaled to our reference volume to allow a direct comparison.

The multicomponent SANS data in Figure 8 is presented in the form of a Zimm plot in Figure 12a. It is evident that the data can be fit with linear expressions, as shown by the solid lines. Extrapolation of these fits for data at each  $P$  to  $q = 0 \text{ nm}^{-1}$

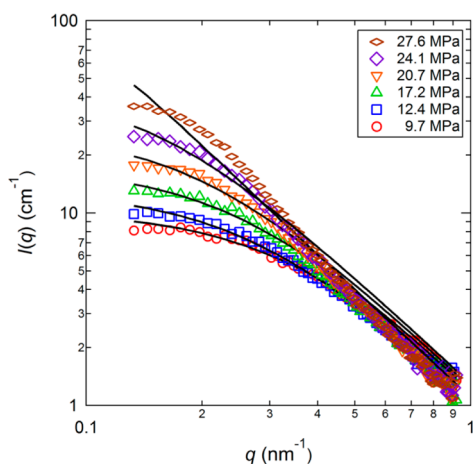


**Figure 8.** Small-angle neutron scattering results for the blend of  $\text{scCO}_2/\text{SAN77(26)}/\text{dPMMA125}$  ( $\phi_{3,0} = 0.461$ ) at 313 K as a function of overall  $P$ . The scattering experiments were performed at 9.7 MPa (red circles), 12.4 MPa (blue squares), 17.2 MPa (green triangles), 20.7 MPa (orange inverted triangles), 24.1 MPa (purple diamonds), and 27.6 MPa (brown rhombi). The solid lines are multicomponent random phase approximation fits to the data with  $\chi_{13}$  and  $\alpha$  as adjustable parameters. Error bars on the SANS data points representing one standard deviation in the measured intensity are within the size of the data symbols.

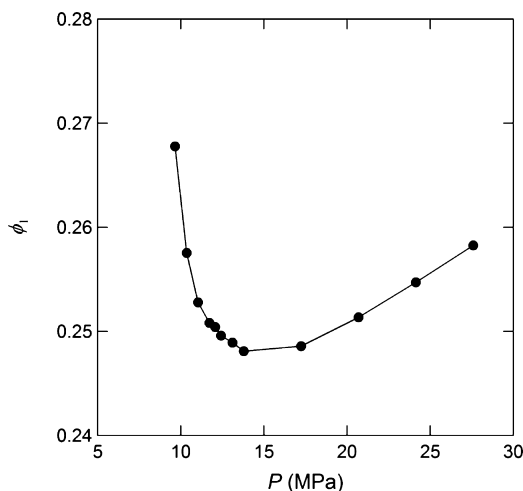


**Figure 9.** Predicted volume fraction of  $\text{scCO}_2$  ( $\phi_1$ ) at 313 K in a blend of  $\text{SAN77(26)}$  and  $\text{dPMMA125}$  containing  $\phi_{3,0} = 0.461$  ( $\text{scCO}_2$ -free volume fraction) as a function of  $P$ .

yields values of  $I_{0,\text{Zimm}}$ . In addition, the RPA fits to the data were extrapolated to  $q = 0$  to obtain  $I_{0,\text{RPA}}$ . In Figure 12b, we plot  $1/I_{0,\text{Zimm}}$  and  $1/I_{0,\text{RPA}}$  versus  $P$ . It is evident that  $1/I_{0,\text{Zimm}}$  and  $1/I_{0,\text{RPA}}$  are linear functions of  $P$ . The pressure at which phase separation is expected ( $P_s$ ) is obtained by extrapolating the lines in Figure 12b to meet the abscissa. The Zimm analysis predicts  $P_s = (29 \pm 1)$  MPa, while the RPA analysis predicts  $P_s = (27 \pm 4)$  MPa. The experimentally determined value of  $P_s$  is  $(30 \pm 2)$  MPa. These values are in agreement within error. We note in passing that there has been considerable interest in the effect of  $\text{scCO}_2$  on homopolymers and polymer blends in the vicinity of its critical point due to the anomalous increase in swelling of polymers in this regime.<sup>37,38</sup> The phase separation that we observe in our  $\text{scCO}_2/\text{SAN}/\text{dPMMA}$  blend occurs at  $P$  well-removed from the  $P_{c,\text{CO}_2}$  which leads us to conclude that

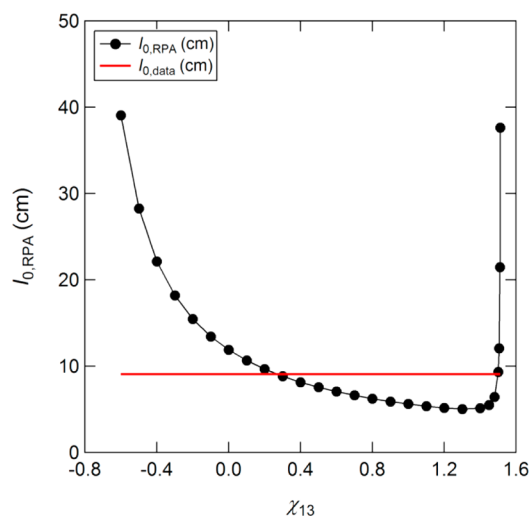


**Figure 10.** Values of the SANS intensity extrapolated to  $q = 0 \text{ nm}^{-1}$ ,  $I_0$ , predicted by multicomponent RPA expressions ( $I_{0,\text{RPA}}$ ) are shown as a function of the single independent interaction parameter,  $\chi_{13}$ , for  $T = 313 \text{ K}$  and  $P = 9.7 \text{ MPa}$ . The experimentally determined value of  $I_0$  ( $I_{0,\text{data}}$ ), obtained by Zimm-style ( $1/I$  vs  $q^2$ ) extrapolation of the data, is shown as a horizontal line. The values of  $\chi_{13}$  which meet the condition of  $I_{0,\text{RPA}} = I_{0,\text{data}}$  (i.e.,  $\chi_{13} = 0.269$  and  $1.499$ ) are both consistent with the experimental results.

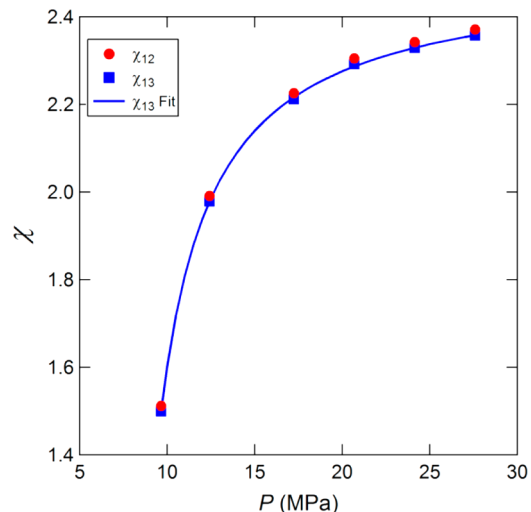


**Figure 11.** Flory–Huggins parameters  $\chi_{1i}$ , where  $i$  refers to the polymeric components of the ternary blend  $\text{scCO}_2/\text{SAN77(26)}/\text{dPMMA125}$ , as a function of pressure at  $T = 313 \text{ K}$  (component 1 =  $\text{scCO}_2$ , component 2 =  $\text{SAN77(26)}$ , component 3 =  $\text{dPMMA125}$ ). The results are obtained from multicomponent random phase approximation fits of small-angle neutron scattering data measured while  $\text{scCO}_2$  loading was increased *in situ*. An empirical function describing the dependence of  $\chi_{13}$  on  $P$  is shown as a solid line. The error bars for each  $\chi_{1i}$  represent one standard deviation in the measured value and are within the size of the data symbols in this figure.

the phase transition occurs due to changes in the delicate balance of interaction energies of the three components, rather than inherent nature of  $\text{scCO}_2$  to experience dramatic density fluctuations near the so-called “density-fluctuation ridge”.

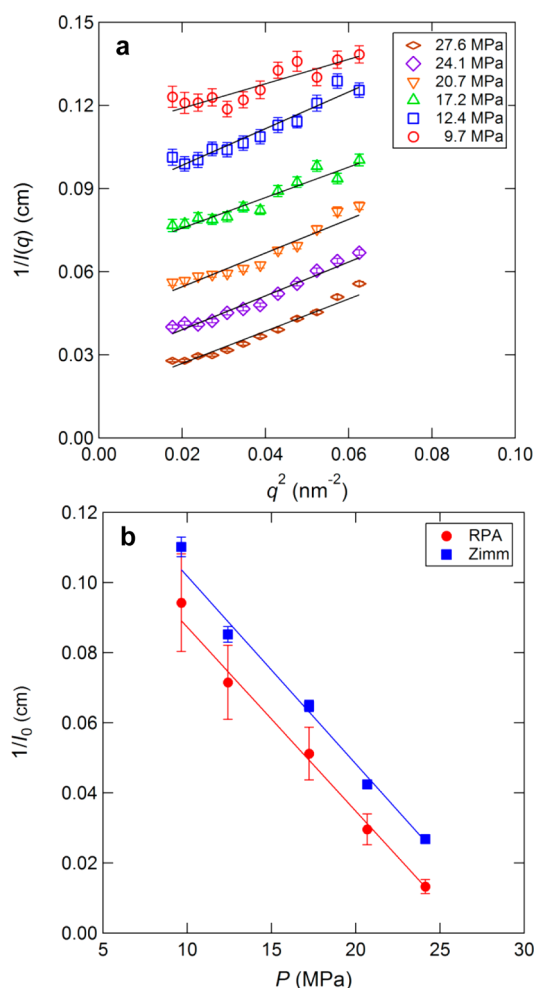


**Figure 12.** (a) Reciprocal of the absolute scattering intensity,  $1/I$ , plotted against  $q^2$ . Least-squares linear fits to the data are shown with solid lines. (b) Reciprocal of the absolute scattering intensity at  $q = 0 \text{ nm}^{-1}$ ,  $1/I_0$ , as a function of  $P$ . The  $P$ -dependence of  $1/I_0$  was found both by extrapolating the random phase approximation fit to  $q = 0 \text{ nm}^{-1}$  (RPA, red circles), and by using the Zimm format ( $1/I$  vs  $q^2$ ) to determine  $1/I(q = 0)$  (Zimm, blue squares). The pressure at which  $1/I_0 = 0$  can be considered the phase separation pressure,  $P_s$ , which is found by least-squares linear fit to the data, shown as solid lines. Using the two methods provides values for  $P_s$  for the blend at  $T = 313 \text{ K}$  with reasonable agreement:  $P_{s,\text{RPA}} = (27 \pm 4) \text{ MPa}$ , and  $P_{s,\text{Zimm}} = (29 \pm 1) \text{ MPa}$ . The error bars in the figure represent one standard deviation in the value of  $1/I_0$  that was determined from the SANS measurements.

## 5. CONCLUSIONS

We present the first quantitative analysis of SANS data from homogeneous multicomponent mixtures of supercritical carbon dioxide and two polymers. Model polymers with narrow molecular weight distributions were used to facilitate comparisons between theory and experiment. A significant portion of our effort was devoted to the synthesis and characterization of a model high-molecular weight SAN copolymer. A formalism of the random phase approximation was developed for multicomponent blends containing a diluent with widely tunable molecular size. The  $\text{scCO}_2$ -free binary blend was studied to determine the  $T$ -dependence of the polymer–polymer interaction parameter.  $\text{scCO}_2$ -polymer solubility data was used to relate polymer–solvent interaction parameters. The measured SANS profiles from our multi-

component mixtures were in remarkable agreement with predictions based on multicomponent RPA with only two fitting parameters,  $\chi_{13}$  and  $\alpha$ . The 11 other parameters needed to calculate  $I(q)$  (i.e.,  $N_2$ ,  $N_3$ ,  $\nu_1$ ,  $\nu_2$ ,  $\nu_3$ ,  $\phi_1$ ,  $b_1$ ,  $b_2$ ,  $b_3$ ,  $\chi_{23}$ ,  $\chi_{12}$ ) were obtained from independent experiments. In the absence of  $\text{scCO}_2$ , our blend is predicted to exhibit phase separation at  $T = T_s = 440 \text{ K}$ . The addition of  $\text{scCO}_2$  at a modest pressure of 30 MPa results in a decrease of  $T_s$  by 127 K. The multicomponent RPA analysis indicates that the qualitative change in  $T_s$  is caused by an increase in  $\chi_{13}$  (and  $\chi_{12}$ ) with increasing  $\text{scCO}_2$  pressure (Figure 11). Further work is needed to identify the molecular underpinnings of  $\chi_{13}$  determined in the multicomponent blends. The dependence of the measured parameters on blend composition and deuterium labeling will be addressed in future publications.

## ■ ASSOCIATED CONTENT

### Supporting Information

Discussion of high-pressure small-angle neutron scattering experimental set-up and a figure showing scattering length density of the pure components. This material is available free of charge via the Internet at <http://pubs.acs.org>.

## ■ AUTHOR INFORMATION

### Corresponding Author

\*E-mail: (N.P.B.) [nbalsara@berkeley.edu](mailto:nbalsara@berkeley.edu). Telephone: (510) 642-8937.

### Author Contributions

†These two authors equally contributed to this work.

### Notes

The authors declare no competing financial interest.

## ■ ACKNOWLEDGMENTS

We acknowledge The Dow Chemical Company for providing the primary support for this work, and thank Dr. Alan Nakatani and Dr. Tirtha Chatterjee for educational discussions on the design and interpretation of SANS experiments. Dr. Boualem Hammouda, Mr. Cedric Gagnon, and Mr. Juscelino Leao of the NIST Center for Neutron Research are thanked for their assistance in carrying out SANS experiments. Dr. Chris Canlas and Dr. Jeffrey G. Pelton of the University of California, Berkeley are thanked for their help with the NMR measurements. We acknowledge the support of the National Institute of Standards and Technology, U.S. Department of Commerce, in providing the neutron research facilities used in this work. This work utilized facilities supported in part by the National Science Foundation under Agreement No. DMR-0454672. Work at the Molecular Foundry was supported by the Office of Science, Office of Basic Energy Sciences, of the U.S. Department of Energy under Contract No. DE-AC02-11231.

## ■ NOMENCLATURE

### Abbreviations

AN	acrylonitrile
ARGET ATRP	activators regenerated by electron transfer ATRP
ATRP	atom-transfer radical polymerization
$\text{CDCl}_3$	deuterated chloroform
CRP	controlled radical polymerization
$\text{CuCl}_2$	copper(II) chloride
dPMMA	deuterated poly(methyl methacrylate) homopolymer

EBiB	ethyl 2-bromo isobutyrate
FT-IR	Fourier-transform infrared
GPC	gel permeation chromatography
hPMMA	hydrogenous poly(methyl methacrylate) homopolymer
LCST	lower critical solution temperature
Me <sub>6</sub> TREN	tris[2-(dimethylamino)ethyl]amine
PDI	polydispersity index
PMMA	poly(methyl methacrylate) homopolymer
RPA	random phase approximation
S	styrene
SAN	styrene-acrylonitrile random copolymer
SANS	small-angle neutron scattering
scCO <sub>2</sub>	supercritical carbon dioxide
Sn(EH) <sub>2</sub>	tin(II) 2-ethylhexanoate
THF	tetrahydrofuran
UCST	Upper critical solution temperature

### Symbols

$A_1$	constant in eq 22
$A_2$	constant in eq 22
$B$	neutron scattering length contrast, nm <sup>-2</sup>
$b$	neutron scattering length, nm
$C$	constant in eq 23
$D$	constant in eq 23, K
$I(q)$	coherent scattered neutron intensity, cm <sup>-1</sup>
$I_0$	scattering intensity extrapolated to $I(q = 0 \text{ nm}^{-1})$ , cm <sup>-1</sup>
$G_m$	free energy density of mixing, J/nm <sup>3</sup>
$k$	Boltzmann constant, $1.38 \times 10^{-23}$ J/K
$l$	statistical segment length, nm
$l_{\text{ref}}$	statistical segment length at $T_{\text{ref}}$ and $P_{\text{ref}}$ , nm
$M_0$	monomer molecular weight, kg/mol
$M_n$	number-averaged molecular weight, kg/mol
$M_w$	weight-averaged molecular weight, kg/mol
$N$	number of monomer units in a chain
$N^*$	number of effective monomer units of size 0.1 nm <sup>3</sup> in a given chain
$N_{\text{AVE}}^*$	average value of $N^*$ for two polymers in binary blend
$P$	pressure, MPa
$P_{\text{c,CO}_2}$	critical pressure of CO <sub>2</sub> , 7.38 MPa
$P_i(q)$	single-chain form factor for species $i$
$P_{\text{ref}}$	reference pressure, 0.1 MPa
$q$	scattering vector, nm <sup>-1</sup>
$R$	ideal gas constant, 8.314 J/mol-K
$R_g$	radius of gyration of species $i$ , nm
$S_{ij}(q)$	complete structure factor for species $i$ and $j$ , nm
$S_{ij}^p(q)$	partial structure factor for species $i$ and $j$ , nm
$T$	absolute temperature, K
$T_{\text{c,CO}_2}$	critical temperature of CO <sub>2</sub> , 304.1 K
$T_g$	glass transition temperature, K
$T_{\text{ref}}$	reference temperature, 413.15 K
$V_{ij}(q)$	interaction structure factor for species $i$ and $j$ , nm
$v$	monomer volume for species $i$ , nm <sup>3</sup>
$v_0$	monomer unit reference volume, 0.1 nm <sup>3</sup>
$w$	blend weight fraction
$w_{\text{AN}}$	copolymer composition in weight fraction acrylonitrile monomer

### Greek

$\alpha$	chain expansion factor
$\theta$	scattering angle, rad
$\lambda$	neutron wavelength, nm
$\mu$	chemical potential in mixture, J/mol
$\mu^\circ$	chemical potential of pure component, J/mol

$\phi$	blend volume fraction
$\phi_{\text{crit}}$	critical volume fraction of species $i$
$\chi$	Flory–Huggins interaction parameter for species $i$ and $j$

**Subscripts**

$i$	blend constituent species (1 = scCO <sub>2</sub> , 2 = SAN, 3 = PMMA)
1– $i$	scCO <sub>2</sub> in a binary mixture with $i = 2$ (SAN) or 3 (PMMA)
$s$	condition for phase separation

### REFERENCES

- (1) DeSimone, J. M.; Guan, Z.; Elsbernd, C. S. *Science* **1992**, *257*, 945–947.
- (2) Amonoo, J. A.; Glynos, E.; Chen, X. C.; Green, P. F. *J. Phys. Chem. C* **2012**, *116*, 20708–20716.
- (3) Xu, G.; Wang, N.; Wei, J.; Lv, L.; Zhang, J.; Chen, Z.; Xu, Q. *Ind. Eng. Chem. Res.* **2012**, *51*, 14390–14398.
- (4) Dutriez, C.; Satoh, K.; Kamigaito, M.; Yokoyama, H. *RSC Adv.* **2012**, *2*, 2821–2827.
- (5) Gong, P.; Ohshima, M. *J. Polym. Sci. B: Polym. Phys.* **2012**, *50*, 1173–1180.
- (6) Jacobs, L. J. M.; Kemmere, M. F.; Keurentjes, J. T. F. *Green Chem.* **2008**, *10*, 731–738.
- (7) Costeux, S.; Bunker, S. P.; Jeon, H. K. *J. Mater. Res.* **2013**, DOI: 10.1557/jmr.2013.100.
- (8) Melnichenko, Y. B.; Kiran, E.; Wignall, G. D.; Heath, K. D.; Salaniwal, S.; Cochran, H. D.; Stamm, M. *Macromolecules* **1999**, *32*, 5344–5347.
- (9) Watkins, J. J.; Brown, G. D.; RamachandraRao, V. S.; Pollard, M. A.; Russell, T. P. *Macromolecules* **1999**, *32*, 7737–7740.
- (10) Vogt, B. D.; Watkins, J. J. *Macromolecules* **2002**, *35*, 4056–4063.
- (11) RamachandraRao, V. S.; Vogt, B. D.; Gupta, R. R.; Watkins, J. J. *J. Polym. Sci. B: Polym. Phys.* **2003**, *41*, 3114–3126.
- (12) Walker, T. A.; Melnichenko, Y. B.; Wignall, G. D.; Spontak, R. J. *Macromolecules* **2003**, *36*, 4245–4249.
- (13) Walker, T. A.; Melnichenko, Y. B.; Wignall, G. D.; Lin, J. S.; Spontak, R. J. *Macromol. Chem. Phys.* **2003**, *204*, 2064–2077.
- (14) Walker, T. A.; Colina, C. M.; Gubbins, K. E.; Spontak, R. J. *Macromolecules* **2004**, *37*, 2588–2595.
- (15) Fowler, M. E.; Barlow, J. W.; Paul, D. R. *Polymer* **1987**, *28*, 1177–1184.
- (16) Tsarevsky, N. V.; Sarbu, T.; Goebelt, B.; Matyjaszewski, K. *Macromolecules* **2002**, *35*, 6142–6148.
- (17) Tsarevsky, N. V.; Bernaerts, K. V.; Dufour, B.; Du Prez, F. E.; Matyjaszewski, K. *Macromolecules* **2004**, *37*, 9308–9313.
- (18) Jakubowski, W.; Min, K.; Matyjaszewski, K. *Macromolecules* **2006**, *39*, 39–45.
- (19) Pietrasik, J.; Dong, H.; Matyjaszewski, K. *Macromolecules* **2006**, *39*, 6384–6390.
- (20) Certain commercial equipment, instruments, materials, and suppliers are identified in this paper to foster understanding. Such identification does not imply recommendation or endorsement by the National Institute of Standards and Technology, nor does it imply that the materials or equipment identified are necessarily the best available for the purpose.
- (21) Eitouni, H. B.; Balsara, N. P. In *Physical Properties of Polymers Handbook*, 2nd ed.; Mark, J. E., Ed.; AIP Press: Woodbury, NY, 2007; p 339.
- (22) Wen, G.; An, L. *J. Appl. Polym. Sci.* **2003**, *90*, 959–962.
- (23) Kline, S. R. *J. Appl. Crystallogr.* **2006**, *39*, 895–900.
- (24) Balsara, N. P.; Lohse, D. J.; Graessley, W. W.; Krishnamoorti, R. *J. Chem. Phys.* **1994**, *100*, 3905–3910.
- (25) de Gennes, P. G. *Scaling Concepts in Polymer Physics*; Cornell University Press: Ithaca, NY, 1979.
- (26) Hammouda, B. *Adv. Polym. Sci.* **1993**, *106*, 87–133.
- (27) Lefebvre, A. A.; Lee, J. H.; Balsara, N. P.; Hammouda, B. *Macromolecules* **2000**, *33*, 7977–7989.
- (28) Lefebvre, A. A.; Balsara, N. P.; Lee, J. H.; Vaidyanathan, C. *Macromolecules* **2002**, *35*, 7758–7764.

- (29) Flory, P. J. *J. Chem. Phys.* **1942**, *10*, 51–61.
- (30) Huggins, M. L. *J. Phys. Chem.* **1942**, *46*, 151–158.
- (31) Nyquist, R. A. *Appl. Spectrosc.* **1987**, *41* (5), 797–800.
- (32) Barron, P. F.; Hill, D. J. T.; O'Donnell, J. H.; O'Sullivan, P. W. *Macromolecules* **1984**, *17*, 1967.
- (33) Personal communication.
- (34) Span, R.; Wagner, W. *J. Phys. Chem. Ref. Data* **1996**, *25*, 1509–1596.
- (35) Condo, P. D.; Sanchez, I. C.; Panayiotou, C. G.; Johnston, K. P. *Macromolecules* **1992**, *25*, 6119–6127.
- (36) Lefebvre, A. A.; Lee, J. H.; Balsara, N. P.; Hammouda, B.; Krishnamoorti, R.; Kumar, S. *Macromolecules* **1999**, *32*, 5460–5462.
- (37) Koga, T.; Seo, Y.-S.; Shin, K.; Zhang, Y.; Rafailovich, M. H.; Sokolov, J. C.; Chu, B.; Satija, S. K. *Macromolecules* **2003**, *36*, 5236–5243.
- (38) Koga, T.; Seo, Y.-S.; Zhang, Y.; Shin, K.; Kusano, K.; Nishikawa, K.; Rafailovich, M. H.; Sokolov, J. C.; Chu, B.; Pfeiffer, D.; Occhiogrosso, R.; Satija, S. K. *Phys. Rev. Lett.* **2002**, *89*, 125506–1–4.